



# Synthesis of Fe<sub>3</sub>O<sub>4</sub>-PVP nanocomposite functionalized with sulfonic group as an effective catalyst for one-pot synthesis of xanthene derivatives

Mohsen Karegar<sup>1</sup> · Mohammad Mehdi Khodaei<sup>1,2</sup>

Received: 27 April 2021 / Accepted: 12 July 2021 / Published online: 3 August 2021  
© The Author(s), under exclusive licence to Springer Nature B.V. 2021

## Abstract

An effective and environmentally friendly Fe<sub>3</sub>O<sub>4</sub>-PVP nanocomposite functionalized with sulfonic group, Fe<sub>3</sub>O<sub>4</sub>-PVP-SO<sub>3</sub>H, was synthesized and characterized as the heterogeneous nanocatalyst for one-pot synthesis of xanthene derivatives via condensation reaction of various aldehydes and dimedone in ethanol media. The catalyst was efficient, and can be separated easily from the reaction mixture and recovered rapidly by an external magnetic field. It can be used five times without significant loss of its activity. Physicochemical properties were characterized using different techniques including FT-IR, XRD, FE-SEM, EDS, TGA, and VSM to illustrate the structure of the catalyst. The presence of sulfonic group on the surface of the catalyst was confirmed by these analyses. Large number of the acidic groups on the surface of the PVP layer led to the more activity of the catalyst and consequently, the yield of xanthene increases. The products were obtained in high yields with short reaction times.

**Keywords** Polyvinylpyrrolidone · Magnetic nanoparticles · Xanthene · Solid acid nanocatalyst

## Introduction

Nanocomposites are a specific class of nano-sized materials that have been applied in different area such as catalysts, drug delivery, cosmetic orthodontics, modern construction, electronics, tissue engineering and agriculture. [1–7]. Magnetic nanocomposites were prepared by modification of magnetic nanoparticles with different

---

✉ Mohammad Mehdi Khodaei  
mmkhoda@razi.ac.ir

<sup>1</sup> Department of Organic Chemistry, Razi University, 67149-67346 Kermanshah, Iran

<sup>2</sup> Nanoscience & Nanotechnology Research Center (NNRC), Razi University, 67149-67346 Kermanshah, Iran

organic and inorganic materials with unique functionality [8]. Iron oxide nanopowder ( $\text{Fe}_3\text{O}_4$ ) is one of the most popular nanoparticles because of its application in ferrofluids [9], high-density information storage [10], magnetic resonance imaging [11] as well as the role of catalyst or support of catalysts [12]. Moreover, in recent years,  $\text{Fe}_3\text{O}_4$  nanoparticles (MNPs) have been attracted in different fields due to their unique properties such as simple synthesis, high surface area, easy separation and recovery from reaction medium using a simple magnet [13–19]. However, MNPs have several problems such as the tendency for aggregation and easily air oxidation because of having high chemical activity on their surface which then cause their magnetic properties and dispersibility to decrease [13, 20–22]. Thus, it is necessary to overcome these problems by chemically stabilization of MNPs via functionalization with different materials such as polymer, silica, carbon, metal oxide and oxide absorber [12, 23–28]. These problems were overcome using one of the promising candidates, polymer coating, which stabilizes MNPs due to its specific characteristics [20, 29–31]. Polymers like PVP can tackle the challenge due to its solubility (soluble in water and polar solvents), stability, low production cost, easy functionalization, and low toxicity. Also, PVP is an excellent stabilizer and has been used for coating of MNPs [32–34]. This polymer made from the monomer N-vinylpyrrolidone that has polar amide group in the ring. These functional groups along their backbones are soluble in many solvents and give them chelating characteristics [35–37]. It was reported that PVP molecules prevent of random agglomeration of iron oxide particles and facilitate the cluster formation [33]. This stabilizer prevents aggregation of MNPs through the repulsive forces due to its hydrophobic carbon chains that disperse within solvents and interact with each other. Moreover, the addition of PVP to MNPs reduces average particle size by preventing agglomeration [38]. The increasing amount of PVP, during chemical reduction synthesis of iron oxide nanoparticles, controls the size and oxidation of the final nanoparticles and changes the final morphology. In addition, crystal growth of iron oxide was restricted in the presence of PVP, and its oxidation limited. Significantly, PVP can apply as a growth modifier, nanoparticle dispersant, and reducing agent related to the particular synthetic conditions [34, 38]. Also, the type of materials and the synthesis method are important for modifying the performance of  $\text{Fe}_3\text{O}_4$  nanoparticles [39]. The uniqueness of the powder with large surface-area is detrimental for the catalytic applications.

Xanthene derivatives constitute an important class of organic oxygen-containing compounds that have been used for pharmaceutical applications possessing antiviral and antibacterial properties [40–42]. In addition, these heterocyclic compounds have been widely used as sensitizers in photodynamic therapy [43], pH sensitive fluorescent materials for visualization of biomolecules [44, 45], and luminescent dyes [46].

In continuation of our ongoing research on using heterogeneous nanocatalyst [47–51] herein, the efficient synthesis of xanthenes catalyzed by  $\text{Fe}_3\text{O}_4$ -PVP- $\text{SO}_3\text{H}$  via one-pot reactions of aldehydes and dimedone was reported. This work was cleanly performed in ethanol as the solvent under reflux conditions. Moderate catalytic activity, catalyst recyclability, easy reaction conditions, simple magnetically catalyst separation and reduction in the amount of acidic waste make the catalyst as an effective green catalyst for the synthesis of xanthene derivatives.

## Experimental

### General

The chemical materials, reagents, and solvents in this research were purchased from Merck and Sigma-Aldrich companies and used without any purification. <sup>1</sup>H NMR and <sup>13</sup>C NMR spectra were recorded on a Bruker 300 MHz spectrometer in CDCl<sub>3</sub> as the solvent. Melting points were determined with Electrothermal 9300 (Electrothermal, Essex, UK). FT-IR BRUKER, Model tensor 27 spectrometer was applied to record IR spectra of all samples with a scanning range of 400–4000 cm<sup>-1</sup> with using KBr pellets. X-ray diffraction (XRD) patterns were obtained by a Philips X-ray analytical diffractometer using Cu/Kα radiation at room temperature in the range of 2θ from 10 to 80° to prove the catalyst contents. VSM spectrum was obtained by a vibrating-sample magnetometer (VSM, LBKFB model-Meghnatis Daghigh Kavir Company) at room temperature and measured the magnetic properties of the catalyst. Thermogravimetric analysis (TGA) was carried out by Bahr STA 503 thermal analysis system heated from 25 to 500 °C using a heating rate of 10 °C /min under N<sub>2</sub> flow. Field emission scanning electron microscopy (FE-SEM) images and energy-dispersive X-ray (EDX) analysis of samples were obtained with a TESCAN MIRA3 digital scanning microscope and Bruker XFlash6130 to determine the morphology and location the elements of the catalyst, respectively. The size, shape and morphology features of nanocomposite were identified using TEM Philips EM 208S and HR-TEM FEI TECNAI F20. Plasma atom emission spectrometer (Perkin-Elmer, DV-530) was used to present the chemical composition of the Fe<sub>3</sub>O<sub>4</sub>-PVP-SO<sub>3</sub>H composite.

### Synthesis of Fe<sub>3</sub>O<sub>4</sub>-PVP nanocomposites

The Fe<sub>3</sub>O<sub>4</sub> NPs were produced with modification according to the previously reported method [52]. At the room temperature, 0.54 g of FeCl<sub>3</sub>·6H<sub>2</sub>O (2 mmol) was dissolved in 25 mL of ethylene glycol, in the presence of N<sub>2</sub> gas to remove oxygen. Then, 0.04 g of CTAB (0.108 mmol) and 0.23 g of PVP (0.0057 mmol) were added into the above solution, respectively. The solution color was changed from yellow to green. Next, 10 mL of the aqueous solution of NaOH (0.2 M) was added to the solution, resulting in a darker solution. Then, the solution was heated to 100 °C under stirring and 0.322 g of sodium citrate (1.25 mmol) as a reducing agent added to the solution. The temperature of the solution was increased to 140 °C under the mechanical stirring vigorously for 24 h. After the reaction was complete, the reaction mixture was allowed to cool for collecting the iron oxide powders using an external magnetic field. The black iron oxide precipitate was washed thoroughly with ethanol two times and dried overnight under vacuum desiccator at room temperature (Fig. S1). To understand and observe the effect of PVP and CTAB on the structure and morphology of Fe<sub>3</sub>O<sub>4</sub> nanoparticles, the iron

oxide nanoparticles without the PVP and CTAB capping agents have been also synthesized using the same procedure.

### Synthesis of Fe<sub>3</sub>O<sub>4</sub>-PVP-SO<sub>3</sub>H nanocomposite

To a suspension solution of 0.6 g Fe<sub>3</sub>O<sub>4</sub>-PVP nanocomposite in 15 mL CH<sub>2</sub>Cl<sub>2</sub>, a solution of 0.15 mL chlorosulfonic acid (2.2 mmol) in 10 mL CH<sub>2</sub>Cl<sub>2</sub> was added and the mixture stirred for 2 h at room temperature. The obtained precipitate was filtered by an external magnet and washed two times with CH<sub>2</sub>Cl<sub>2</sub> (2 × 10 mL). The black powder was produced after drying it in a vacuum desiccator at room temperature.

### Measuring the acidity of the catalyst

To determine the number of SO<sub>3</sub>H groups on the catalyst, the Fe<sub>3</sub>O<sub>4</sub>-PVP-SO<sub>3</sub>H (0.1 g) was added to an aqueous solution of NaOH (10 mL, 0.2 M) in an Erlenmeyer flask. Then the system was stirred for 1 h at room temperature. The catalyst was then removed using an outer magnet and to the resulted a clear solution, two drops of phenolphthalein indicator added. The solution was titrated to a neutrality point using 17.7 mL of an aqueous HCl solution (0.1 M). The blank titration (without adding the catalyst) was also carried out and the volume of used HCl solution (0.1 M) found to be 20 mL. Therefore, the volume of used HCl solution (0.1 M) for computing the number of SO<sub>3</sub>H groups on the catalyst was observed to be 2.3 mL. The H<sup>+</sup> loading of the nanocatalyst can be computed based on Eq. 1:

$$M_1 \times V_1 = M_2 \times V_2, \quad (1)$$

in which M<sub>1</sub> (mol. L<sup>-1</sup>) and V<sub>1</sub> (L) are the used concentration and volume of the NaOH solution (0.2 M), respectively, and M<sub>2</sub> (mol. L<sup>-1</sup>) and V<sub>2</sub> (L) are the used concentration and volume of the HCl solution (0.1 M), respectively, in the titration process. Therefore;

$$V_{\text{cal}} = 20 - 17.7 = 2.3\text{ml}(\text{the acidity rate of the catalyst})$$

$$H_{\text{loading}}^+ = 2.3\text{ml} \times 0.1\text{M} = 0.23\text{mmol}(\text{in the } 0.1\text{g of catalyst})$$

$$H_{\text{loading}}^+ = \frac{0.23\text{mmol} \times 1\text{g}}{0.1\text{g}} = 2.3\text{mmol.g}^{-1}$$

### General procedure for preparation of xanthene derivatives

A mixture of aldehyde (1 mmol), dimedone (2 mmol) and Fe<sub>3</sub>O<sub>4</sub>-PVP-SO<sub>3</sub>H nanocomposite (30 mg) as the catalyst was stirred in 2 mL ethanol at 80 °C under reflux condition. The progress of the reaction was continuously monitored by TLC: ethyl acetate/n-hexane (1:5). After completion of the reaction, the catalyst was separated by an external magnet. Then, the mixture was cooled to room temperature and 5 mL

of ice water added drop by drop and decanted to isolate the crude product. The crude product was put in the oven at 80 °C till dried. The resulting solid as the crude product was recrystallized from EtOH to afford the pure product. The obtained products were characterized by m.p., <sup>1</sup>H NMR, and <sup>13</sup>C NMR techniques.

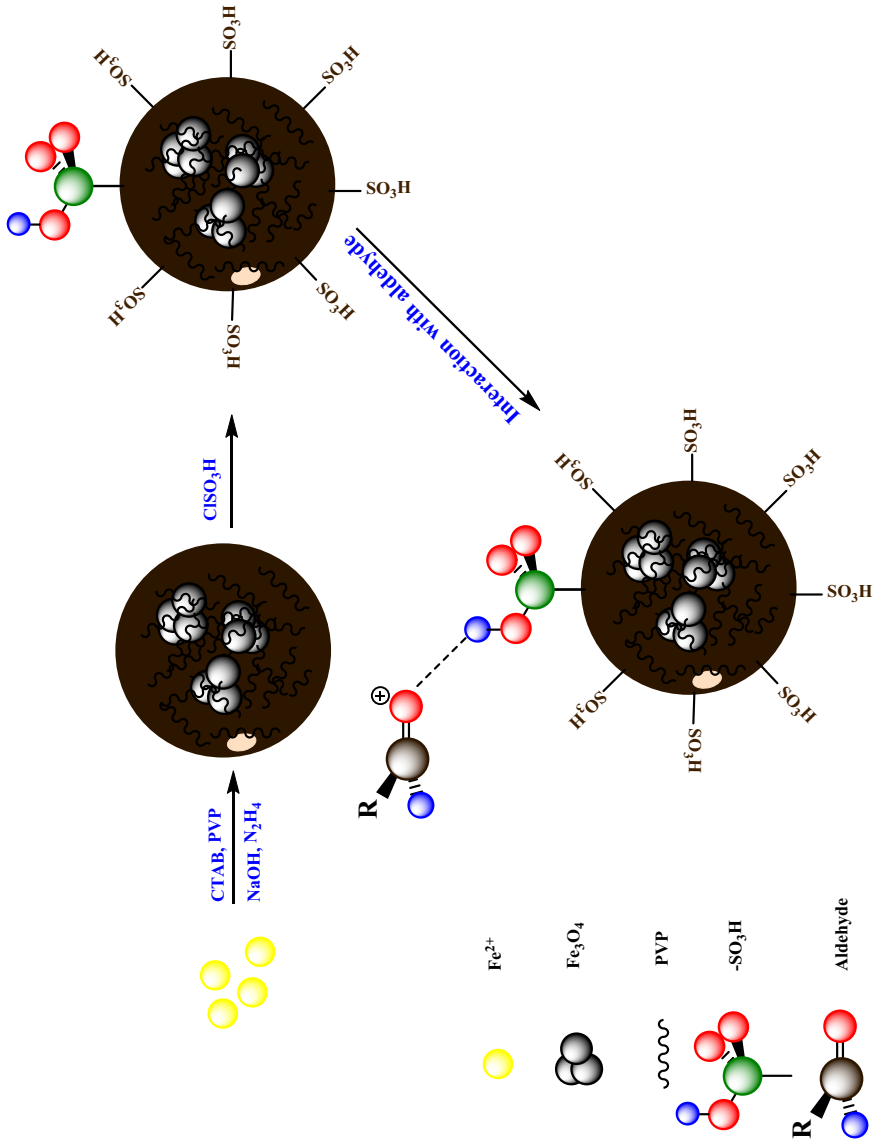
## Results and discussion

### Preparation and characterization of Fe<sub>3</sub>O<sub>4</sub>-PVP-SO<sub>3</sub>H nanocomposite

The polyol process was used for the preparation of iron oxide nanopowders due to create iron oxide nanoparticles of high magnetization and hydrophilic surfaces [32, 53]. In this study, the effects of PVP and CTAB were evaluated on the synthesis of MNPs. It was observed that CTAB and PVP as the coating and stabilizer agents changed MNPs morphology and protected them from oxidation. It is interesting to note that PVP chains cannot interact with MNPs due to their neutral charge and hydrophilic properties, while CTAB can interact easier than PVP with MNPs because it is a cationic surfactant. Moreover, CTAB was converted to cetyltrimethylammonium hydroxide (CTAOH) by alkaline environment during the synthesis [54]. This interaction resulted in smaller crystallite sizes, as well as prevented from oxidation and agglomeration of MNPs [39, 55]. Thus, MNPs were synthesized in the presence of both PVP and CTAB and well protected from agglomeration and oxidation (Figs. 2b and 4a). The preparation of Fe<sub>3</sub>O<sub>4</sub>-PVP-SO<sub>3</sub>H nanocomposite as the solid acid nanocatalyst was depicted in Scheme 1.

**FT-IR** The presence of key functional groups was ascertained through FT-IR spectroscopy. The FT-IR spectra of PVP, Fe<sub>3</sub>O<sub>4</sub>-PVP and Fe<sub>3</sub>O<sub>4</sub>-PVP-SO<sub>3</sub>H have been presented in Fig. 1. The FT-IR spectrum of PVP (Fig. 1a) indicates the bands around 3458 and 1658 cm<sup>-1</sup> that are denoted to hydroxyl and carbonyl groups in PVP while the bands located at 1423 and 1288 cm<sup>-1</sup> related to bending vibration of CH<sub>2</sub> groups and stretching vibration of the C-N bond of PVP, respectively, [56, 57]. The spectrum of Fe<sub>3</sub>O<sub>4</sub>-PVP (Fig. 1b) shows a new strong band at 584 cm<sup>-1</sup> attributed to Fe-O stretching vibration and the peak 1658 shifted to 1649 cm<sup>-1</sup> indicating the interaction among Fe<sub>3</sub>O<sub>4</sub> and PVP. The FT-IR spectrum of Fe<sub>3</sub>O<sub>4</sub>-PVP-SO<sub>3</sub>H (Fig. 1c) shows the appearance extra absorbance peaks at 1074 and 1230 cm<sup>-1</sup>, corresponding to the stretching vibrations of the S-O of sulfonic acid groups [58]. Also, a moderate peak at 1639 cm<sup>-1</sup> which denoted to the imine groups in catalyst is appeared. The obtained results from FT-IR spectra confirm that SO<sub>3</sub>H groups have functionalized on the surface of the Fe<sub>3</sub>O<sub>4</sub>-PVP nanocomposite.

**SEM** The surface morphology was characterized and the fundamental physical properties of the surface were analyzed by scanning electron microscopy (SEM) (Fig. 2). Cheng et al. [32] showed that iron oxide particle size and its dispersion are controlled by tuning the concentration of sodium citrate and adjusting the electrostatic repulsion between particles in the polyol synthesis of iron oxide powders. They concluded by TEM images that the particle size decreased and the particles became loosely packed when, the amount of sodium citrate was increased. Also, Graeve et al. indicated that the small amount of PVP had the similar effect as the



**Scheme 1** The schematic representation for the preparation of  $\text{Fe}_3\text{O}_4/\text{PVP-SO}_3\text{H}$  nanocomposite

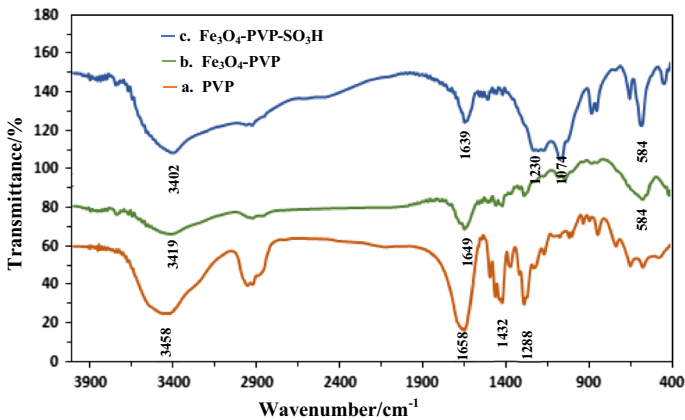
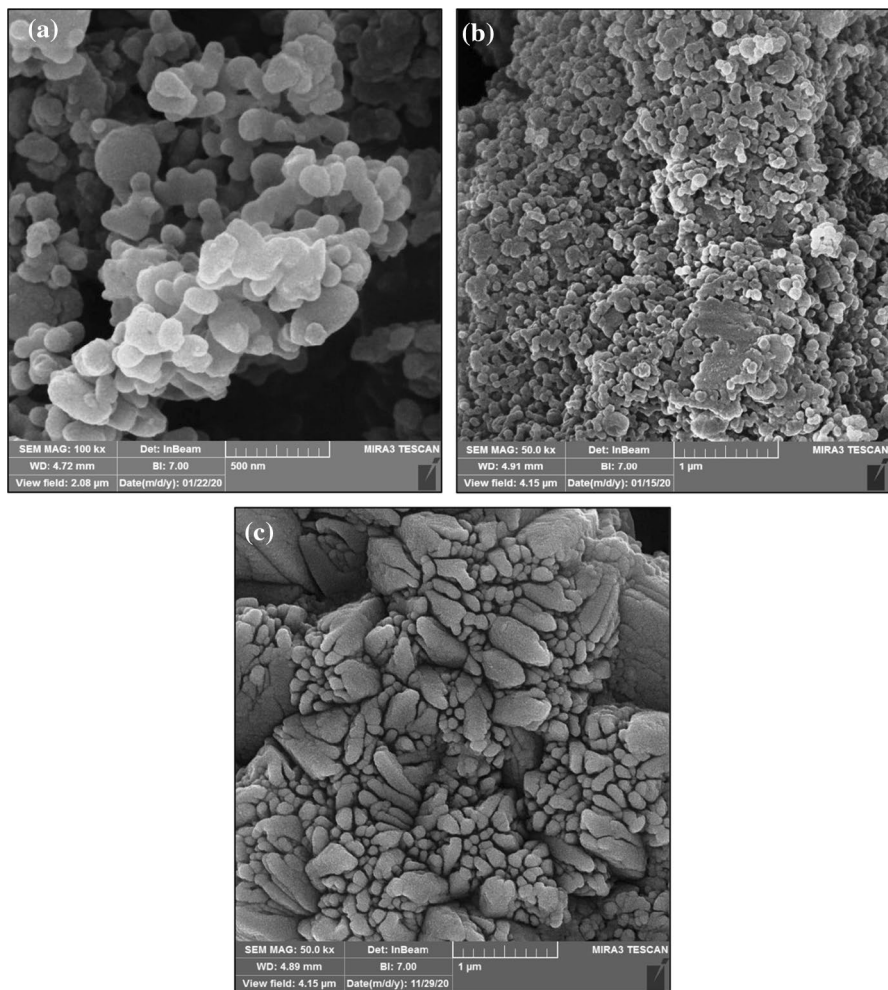


Fig. 1 The FT-IR spectra of (a) PVP, (b) Fe<sub>3</sub>O<sub>4</sub>-PVP and (c) Fe<sub>3</sub>O<sub>4</sub>-PVP-SO<sub>3</sub>H

effect of sodium citrate in Cheng et al.'s work [39]. In our study, the obtained SEM image of Fe<sub>3</sub>O<sub>4</sub>-PVP nanocomposites (Fig. 2b) not only clearly describes the presence of PVP and CTAB decreased the particle size but, also shows that these nanocomposites have a spherical morphology with loosely packed surfaces, confirming the uniformly coating of PVP as protective layer on the Fe<sub>3</sub>O<sub>4</sub> particles. The Stabilizer has been widely applied to control the size and morphology of nanocrystals due to its great effect on the growth of nanocrystals in the synthesis process. According to Fig. 2c, Fe<sub>3</sub>O<sub>4</sub>-PVP-SO<sub>3</sub>H nanocomposites did not keep the morphological properties of Fe<sub>3</sub>O<sub>4</sub>-PVP and lost their spherical morphology due to the little aggregation of the nanocomposites upon addition of chlorosulfonic acid.

## TEM and HR-TEM

Figure 3 shows the TEM and HR-TEM images of the Fe<sub>3</sub>O<sub>4</sub>-PVP-SO<sub>3</sub>H nanocomposite synthesized through electrostatic interactions between cetyltrimethylammonium bromide (CTAB) stabilized Fe<sub>3</sub>O<sub>4</sub> nanoparticles and PVP chains by the polyol process and then modified by the addition of chlorosulfonic acid. Figure 3a, b indicates layers of the continuous network of the PVP on the Fe<sub>3</sub>O<sub>4</sub> nanoparticles surface so that they look much brighter than Fe<sub>3</sub>O<sub>4</sub> nanoparticles. Evidently, the spherical magnetic nanoparticles are observed by dark spots and some of them are shown more dark seem to be agglomerated but, most they are not. However, there are many Fe<sub>3</sub>O<sub>4</sub> nanoparticles with spherical structures who are uniformly dispersed due to the strong interaction between the nanoparticles and the PVP chains. These uniformly dispersed nanoparticles confirm that PVP successfully can prevent of coagulation. To observe the structure with precise detail, the typical HRTEM images of Fe<sub>3</sub>O<sub>4</sub>-PVP-SO<sub>3</sub>H nanocomposite are shown in Fig. 3c, d. The structures of Fe<sub>3</sub>O<sub>4</sub>-PVP-SO<sub>3</sub>H nanocomposite exhibit the crystallinity of Fe<sub>3</sub>O<sub>4</sub> nanoparticles with several spherical shaped nanocrystals in sizes less than 10 nm [39] and amorphous nature of the PVP layer. So that, Fe<sub>3</sub>O<sub>4</sub> NPs were homogenously distributed



**Fig. 2** Scanning electron micrographs of  $\text{Fe}_3\text{O}_4$  NPs synthesized without PVP (a), with PVP (b) and  $\text{Fe}_3\text{O}_4$ -PVP- $\text{SO}_3\text{H}$  nanocomposite (c)

in PVP matrix which resulted to regular arrangement of  $\text{Fe}_3\text{O}_4$  nanoparticles. Furthermore, it must be noted that the SAED pattern with bright spots represented in Fig. 3d can clarify the crystalline nature of  $\text{Fe}_3\text{O}_4$  as indicated by bright spots with uniform diffusive circles.



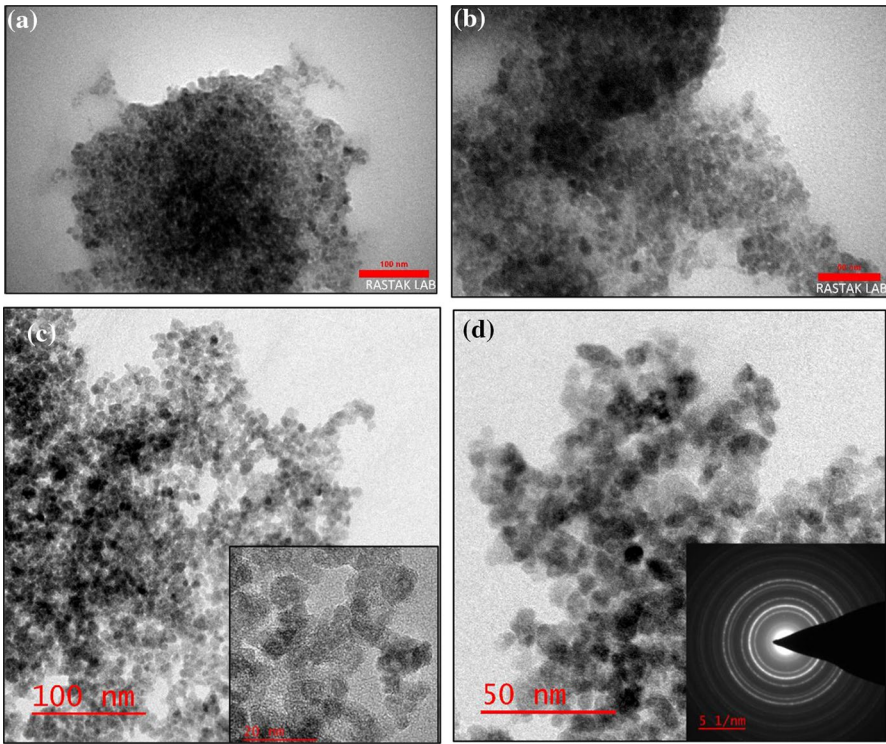


Fig. 3 TEM image (a, b) and HRTEM images of the Fe<sub>3</sub>O<sub>4</sub>-PVP-SO<sub>3</sub>H nanocomposites (c, d)

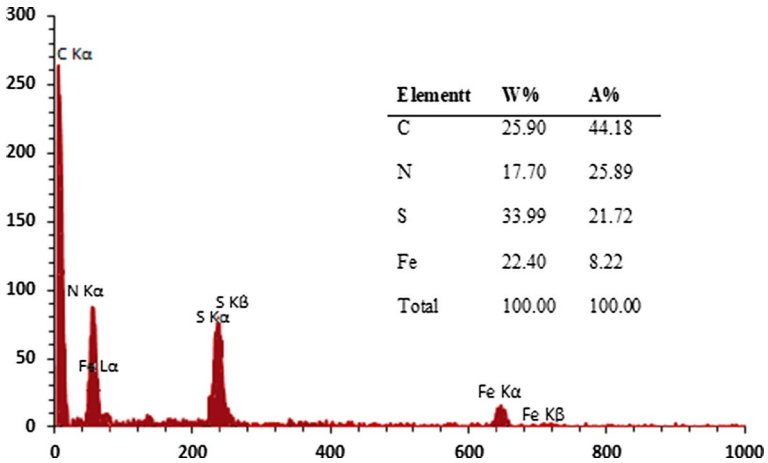


Fig. 4 EDX pattern of Fe<sub>3</sub>O<sub>4</sub>-PVP-SO<sub>3</sub>H nanocomposites

## EDX

EDX is used as a useful technique to determine the elements presented in the nanocomposites. Figure 4 indicates the EDX pattern of  $\text{Fe}_3\text{O}_4$ -PVP- $\text{SO}_3\text{H}$  nanocomposites. This pattern clearly shows the elemental compositions are Fe, N and C and the peaks attributed to S, demonstrating the presence of sulfonic acid group along with PVP in the nanocomposite and the successful synthesis of  $\text{Fe}_3\text{O}_4$ -PVP- $\text{SO}_3\text{H}$  nanocatalyst.

## XRD

XRD analysis was used in order to investigate the crystallographic structure of the catalyst. XRD patterns of  $\text{Fe}_3\text{O}_4$ -PVP and  $\text{Fe}_3\text{O}_4$ -PVP- $\text{SO}_3\text{H}$  are shown in Fig. 4. The XRD of pure PVP indicates the amorphous nature of the polymer owing to appearance of a broad diffraction peak at  $2\theta = 11$  and  $21^\circ$  (Fig. 5a) [59, 60]. The pattern of  $\text{Fe}_3\text{O}_4$ -PVP (Fig. 4a) indicates the presence of peaks in  $2\theta = 30, 36, 43, 53, 57, 63$  and  $75^\circ$ , that is related to (200), (311), (400), (422), (511), (440) and (511) planes of  $\text{Fe}_3\text{O}_4$  nanoparticles (JCPDS 19-0629) [56, 61, 62]. The broad peak at  $2\theta = 21^\circ$  is related to PVP. It can be seen that the XRD patterns of  $\text{Fe}_3\text{O}_4$ -PVP and  $\text{Fe}_3\text{O}_4$ -PVP- $\text{SO}_3\text{H}$  show the same diffraction patterns indicating that the structure of nanocomposite remained intact during the coating and loading of PVP and  $\text{SO}_3\text{H}$ .

## VSM

The magnetic hysteresis measurement of  $\text{Fe}_3\text{O}_4$ -PVP- $\text{SO}_3\text{H}$  is obtained by VSM with the field sweeping from  $-10,000$  to  $+10,000$  Oe (Fig. 6). As shown in this figure, the

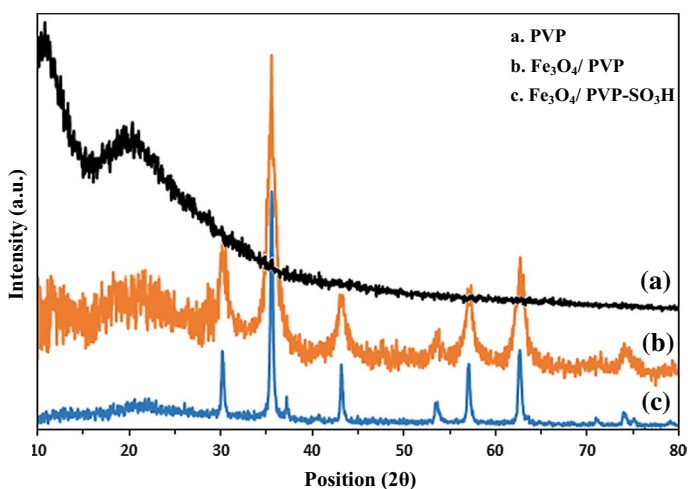
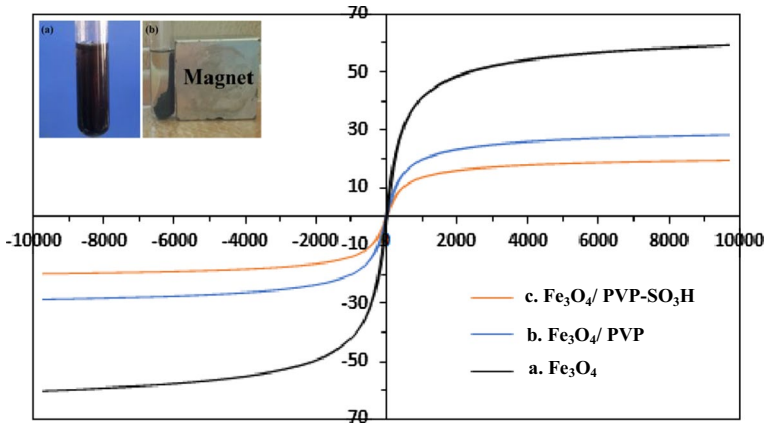


Fig. 5 The X-ray diffraction patterns of (a)  $\text{Fe}_3\text{O}_4$ -PVP and (b)  $\text{Fe}_3\text{O}_4$ -PVP- $\text{SO}_3\text{H}$

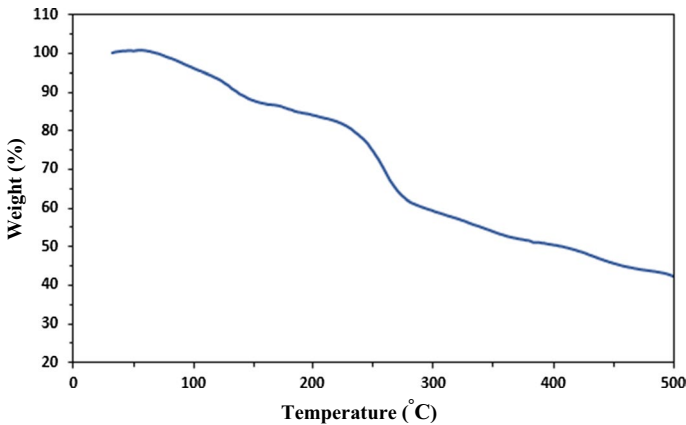


**Fig. 6** Magnetic hysteresis loops of Fe<sub>3</sub>O<sub>4</sub>-PVP-SO<sub>3</sub>H nanocatalyst. The inset indicates the practical model of catalyst separation under an external magnetic field

saturation magnetization values for Fe<sub>3</sub>O<sub>4</sub>, Fe<sub>3</sub>O<sub>4</sub>-PVP and Fe<sub>3</sub>O<sub>4</sub>-PVP-SO<sub>3</sub>H are 61.3, 29.0 and 19.7 emu g<sup>-1</sup>, respectively. The intensity of magnetization of bare Fe<sub>3</sub>O<sub>4</sub> was reduced from 61.3 to 19.7 emu g<sup>-1</sup> because of the increased thickness of grafting by PVP and SO<sub>3</sub>H. The nanocomposites exhibit the superparamagnetic characteristics since the hysteresis loop for the particles was completely reversible. Thus, the Fe<sub>3</sub>O<sub>4</sub>-PVP-SO<sub>3</sub>H can easily separate and recycle from the products using an external magnetic field.

**TGA**

The TGA analysis in the temperature range of 25–500 °C for Fe<sub>3</sub>O<sub>4</sub>-PVP-SO<sub>3</sub>H was shown in Fig. 7. There are three stages of weight losses. The first mass weight loss



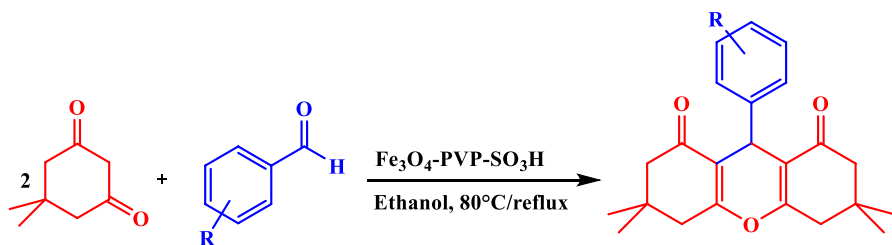
**Fig. 7** Thermogravimetric analysis curve of Fe<sub>3</sub>O<sub>4</sub>-PVP-SO<sub>3</sub>H

(12%) up to 145 °C is assigned exclusively to physically adsorbed water or ethanol molecules on the catalyst surface and the solvent trapped on the surface and /or polymer matrix pores of nanocomposites. The second mass weight loss of 27% was observed at 145–275 °C that can be related to the degradation and decomposition of the sulfonic moieties in  $\text{Fe}_3\text{O}_4\text{-PVP-SO}_3\text{H}$ . The third one with mass weight loss (19.0%) occurred at bigger than 275–500 °C and it is corresponded to PVP decomposition. These results can prove the attachment of sulfonic acid group and PVP moiety onto the surface of  $\text{Fe}_3\text{O}_4$  and show the catalyst has around 58% of organic material. Therefore, it can be concluded that the excellent grafting of PVP and sulfonic groups on the  $\text{Fe}_3\text{O}_4$  exist.

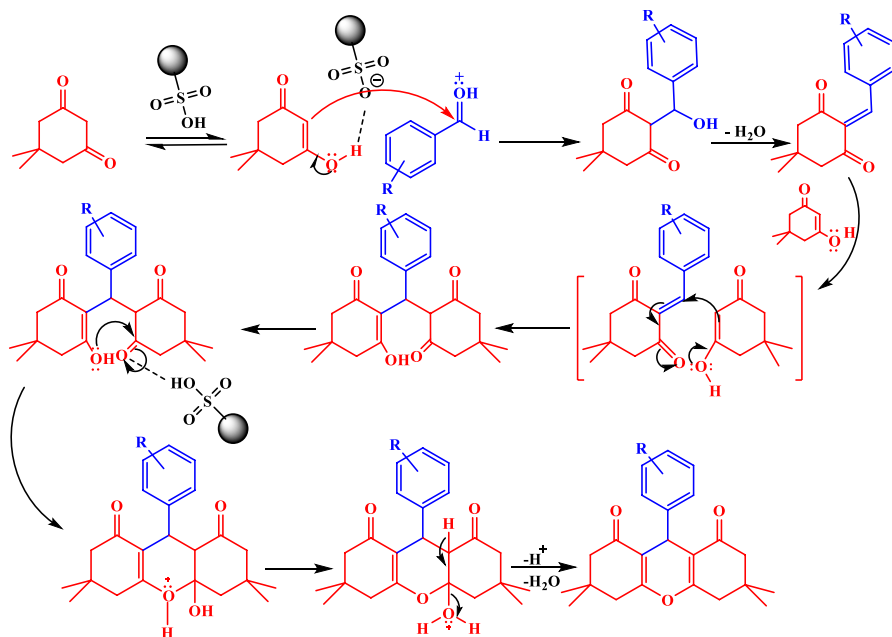
### Investigation of catalytic activity of $\text{Fe}_3\text{O}_4\text{-PVP-SO}_3\text{H}$

The catalytic performance of  $\text{Fe}_3\text{O}_4\text{-PVP-SO}_3\text{H}$  was evaluated in the synthesis of xanthenes derivatives (Scheme 2). To optimize the reaction conditions for synthesis of xanthenes, the effects of the catalyst amount, solvent and temperature were examined. The reaction of benzaldehyde (1 mmol), dimedone (2 mmol), was chosen as a model reaction.

First, the reaction was carried out in solvents including ethanol, acetonitrile, methanol, dimethyl formamide and water under reflux conditions (Table 1, entries 3, 8–11). As indicated in Table 1, ethanol was the best solvent and the xanthenes was obtained in 87% yield after 20 min using 0.03 g of the catalyst. The other solvents were not as effective as EtOH and only gave moderate to low yields of the product. Second, the reaction was heated at different temperatures. It was found that the reflux temperature afforded the best result compared with room temperature and 50 °C (Table 1, entries 5 and 6). This reaction at room temperature even after 60 min gave only trace amount of the product. Finally, to determine the optimum amount of the catalyst, the reaction was examined using 0.02, 0.03 and 0.04 g of the catalyst. Based on the obtained results, the best performance is found when 0.03 g of the catalyst is used. When the amount of the catalyst was increased, the yield of the reaction was slightly raised. It is notable that in the absence of the catalyst the yield of the product was trace (Table 1, entry 1). With the optimal reaction conditions in hand, EtOH as a solvent, reflux temperature, and 0.03 g of the catalyst, the



**Scheme 2** Preparation of xanthenes catalyzed by  $\text{Fe}_3\text{O}_4\text{-PVP-SO}_3\text{H}$  nanocomposite



**Scheme 3** Plausible mechanism for the synthesis of xanthenes in the presence of Fe<sub>3</sub>O<sub>4</sub>-PVP-SO<sub>3</sub>H nanocatalyst

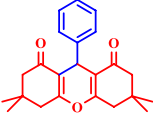
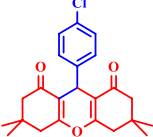
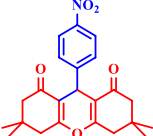

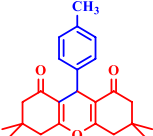

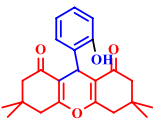
**Table 1** Optimization of the reaction conditions

Entry	Catalyst (g)	Temperature (°C)	Solvent	Time (min)	Yield (%)
1	–	80/Reflux	EtOH	60	Trace
2	Fe <sub>3</sub> O <sub>4</sub> -PVP-SO <sub>3</sub> H (0.02)	80/Reflux	EtOH	40	74
<b>3</b>	<b>Fe<sub>3</sub>O<sub>4</sub>-PVP-SO<sub>3</sub>H (0.03)</b>	<b>80/Reflux</b>	<b>EtOH</b>	<b>20</b>	<b>87<sup>a</sup></b>
4	Fe <sub>3</sub> O <sub>4</sub> -PVP-SO <sub>3</sub> H (0.03)	80/Reflux	EtOH	40	87
5	Fe <sub>3</sub> O <sub>4</sub> -PVP-SO <sub>3</sub> H (0.03)	50	EtOH	20	65
6	Fe <sub>3</sub> O <sub>4</sub> -PVP-SO <sub>3</sub> H (0.02)	r.t	EtOH	60	Trace
7	Fe <sub>3</sub> O <sub>4</sub> -PVP-SO <sub>3</sub> H (0.04)	80/Reflux	EtOH	20	88
8	Fe <sub>3</sub> O <sub>4</sub> -PVP-SO <sub>3</sub> H (0.03)	80	DMF	20	70
9	Fe <sub>3</sub> O <sub>4</sub> -PVP-SO <sub>3</sub> H (0.03)	80	H <sub>2</sub> O	20	45
10	Fe <sub>3</sub> O <sub>4</sub> -PVP-SO <sub>3</sub> H (0.03)	Reflux	CH <sub>3</sub> CN	20	81
11	Fe <sub>3</sub> O <sub>4</sub> -PVP-SO <sub>3</sub> H (0.03)	Reflux	MeOH	20	54
12	Fe <sub>3</sub> O <sub>4</sub> (0.03)	Reflux	EtOH	20	49
13	PVP (0.03)	Reflux	EtOH	20	Trace
14	Fe <sub>3</sub> O <sub>4</sub> -PVP (0.03)	Reflux	EtOH	20	45

<sup>a</sup>Reaction conditions (optimum): benzaldehyde (1 mmol), dimedone (2 mmol), the catalyst (0.03 g), reflux, EtOH, and 20 min.

The reaction proceeded rapidly with functionality substituted aromatic aldehydes with various electron-donating or electron-withdrawing groups such as hydroxyl, methoxy, methyl, chloro and nitro to give the corresponding 1,8-dioxo-octahydroxanthenes in good to high yields. The results are presented in Table 2

**Table 2** Synthesis of xanthene derivatives catalyzed by Fe<sub>3</sub>O<sub>4</sub>-PVP-SO<sub>3</sub>H

Entry	Product	Time (min)	M.P (°C)[ref]/M.P (°C)	Yield <sup>a</sup> (%)
1		20	199–201[63]/ 190–195	87
2		20	227–229[64] 224–226	93
3		20	220–222[64, 65] 218–220	85
4		20	163–165[63] 162–164	74
5		20	213–215[63] 210–212	77
6		20	242–244[64] 244–246	83
7		20	198–200[63] 194–196	81

<sup>a</sup>Reaction conditions: benzaldehyde (1 mmol), dimedone (2 mmol), Fe<sub>3</sub>O<sub>4</sub>-PVP-SO<sub>3</sub>H (0.03 g), EtOH, 80 °C

A plausible mechanism of xanthene derivatives synthesis catalyzed by Fe<sub>3</sub>O<sub>4</sub>-PVP-SO<sub>3</sub>H is indicated in Scheme 3. The Brønsted acidity of the SO<sub>3</sub>H group capable of bonding with the carbonyl oxygen of aldehydes and activated carbon of carbonyl group are shown in Scheme 3

different benzaldehyde derivatives were reacted with dimedone for preparation of various 1,8-dioxo-octahydroxanthenes (Table 2).

To further examine the catalytic behavior of the catalyst for the synthesis of xanthene derivatives, the obtained results were compared with some of those reported in the literature (Table 3). The catalysts of entries 1–4 are homogeneous catalysts

**Table 3** Comparison of Fe<sub>3</sub>O<sub>4</sub>-PVP-SO<sub>3</sub>H with reported catalysts in the synthesis of xanthen derivatives

Entry	Catalyst	Condition	Yield (%), Ref
1	[Et <sub>3</sub> NH][HSO <sub>4</sub> ]	Solvent free, 100 °C	77, [66]
2	[(n-Pr <sub>2</sub> NH <sub>2</sub> )] [HSO <sub>4</sub> ]	Solvent free, 80 °C	85, [67]
3	Cs <sub>2.5</sub> H <sub>0.5</sub> PW <sub>12</sub> O <sub>40</sub>	H <sub>2</sub> O, 100 °C	80, [68]
4	CH <sub>3</sub> CH <sub>2</sub> NH <sub>2</sub> SO <sub>3</sub> HCl	Solvent free, 120 °C	91, [64]
5	Fe(HSO <sub>4</sub> ) <sub>3</sub>	DCM, 25 °C	85, [69]
6	Fe <sub>3</sub> O <sub>4</sub> @SiO <sub>2</sub> -SO <sub>3</sub> H	Solvent free, 110 °C	94, [70]
7	Fe <sub>3</sub> O <sub>4</sub> -PVP-SO <sub>3</sub> H	Ethanol, 80 °C	87, This work

and isolation of them after completion of the reaction are difficult and some of them need higher temperatures for the reactions occur. In addition, they are not recoverable and reusable. Fe(HSO<sub>4</sub>)<sub>3</sub> is robust and heterogeneous catalyst, but its isolation needs filtration which takes time to be isolated. This catalyst was easily separated from the products by exposure of the reaction vessel to an external magnet followed decantation of the reaction solution. The catalyst is energy saving and can be isolated faster without needing filtration. It was found that this catalyst is comparable with the others in terms of the reaction time and yield. Also, due to the magnetic feature of this catalyst, it can be readily separated from the reaction mixture and used at least five times without any noticeable loss of the yield in product.

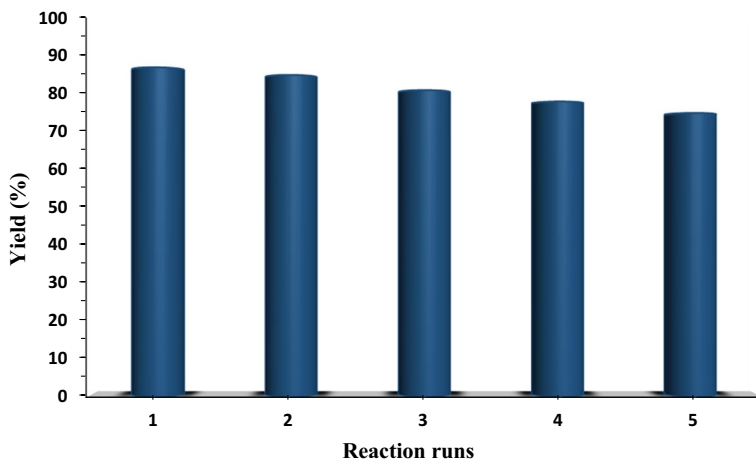
### Leaching test

The hot filtration was carried out to examine the catalyst durability using the model reaction under optimized conditions (Fig S2). The reaction was stopped after 5 min and the catalyst separated from the reaction medium, then the reaction continued in the absence of the catalyst for 20 min. A reaction yield of 25% was found. In another testing, the reaction proceeded for 10 min, then the catalyst was removed from the medium, and the reaction let continue for 20 min in the absence of the catalyst. A yield of 50% was obtained. We believe that the leaching was negligible during the reaction, and after the removal of the catalyst, the reaction was not able to proceed further to a higher yield.

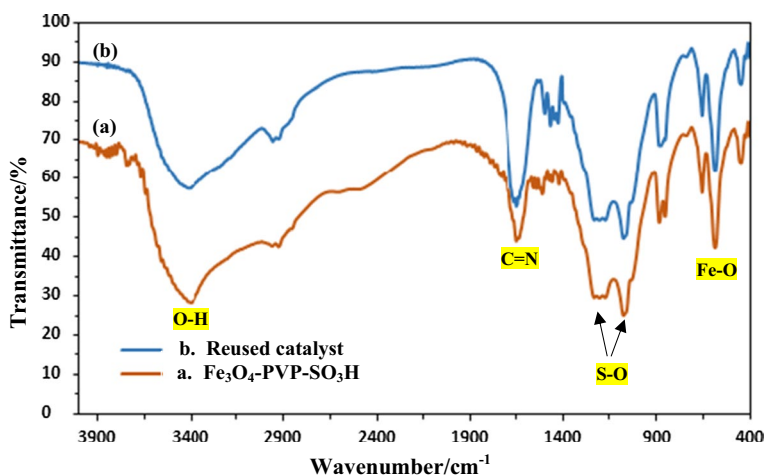
To determine the weight percent of Fe element in the fresh and reused Fe<sub>3</sub>O<sub>4</sub>-PVP-SO<sub>3</sub>H composite, ICP-OES analysis was employed. The weight percent of Fe for the fresh catalyst was calculated to be Fe 7.41%, and in the reused catalyst was 7.24%. The slight decreasing in the element content of Fe indicating unavoidable loss for recycled catalyst after five consecutive runs during the process of collection and washing of the catalyst.

### Recyclability of the catalyst

To consider the stability and recyclability of Fe<sub>3</sub>O<sub>4</sub>-PVP-SO<sub>3</sub>H, after each reaction, the nanocatalyst was separated from the reaction mixture with a magnet, washed



**Fig. 8** Recyclability of Fe<sub>3</sub>O<sub>4</sub>-PVP-SO<sub>3</sub>H nanocatalyst in the synthesis of xanthenes



**Fig. 9** FT-IR spectra of Fe<sub>3</sub>O<sub>4</sub>-PVP-SO<sub>3</sub>H before (a) and after (b) being reused

with water and ethanol, dried under vacuum and reused for another reaction to evaluate its recycling performance. As indicated in Fig. 8, the Fe<sub>3</sub>O<sub>4</sub>-PVP-SO<sub>3</sub>H nanocatalyst can be successfully used for at least five times for synthesis of the xanthenes without significant loss in its catalytic activity. A small decrease in its performance can be ascribed to the loss of the nanocatalyst after every recycling. Furthermore, the FT-IR spectrum of the reused nanocatalyst matches well with the fresh one and it confirms the recoverability and stability of the nanocatalyst during the reactions (Fig. 9).



## Selected spectra data of products

### 3,3,6,6-Tetramethyl-9(phenyl)-1,8-dioxo-octahydroxanthene (Table 2, entry 1)

<sup>1</sup>H NMR (CDCl<sub>3</sub>, 300 MHz), δppm: 0.98 (s, 6H), 1.09 (s, 6H), 2.16 (d, *J*=16.3, 2H), 2.23 (d, *J*=16.3 Hz, 2H), 2.46 (s, 4H), 4.75 (s, 1H), 7.09 (t, *J*=7.0 Hz, 1H), 7.21 (t, *J*=7.0 Hz, 2H), 7.28 (d, *J*=7.20 Hz, 2H); <sup>13</sup>C NMR (CDCl<sub>3</sub>, 75 MHz), δppm: 27.7, 29.6, 32.3, 32.6, 41.3, 51.2, 116.1, 126.8, 128.4, 128.8, 144.5, 162.7, 196.8 ppm.

### 3,3,6,6-Tetramethyl-9(4-chloro-phenyl)-1,8-dioxo-octahydroxanthene (Table 2, entry 2)

<sup>1</sup>H NMR (CDCl<sub>3</sub>, 300 MHz), δppm: 0.98 (s, 6H), 1.09 (s, 6H), 2.14 (d, *J*=16.1 Hz, 2H), 2.23 (d, *J*=16.1 Hz, 2H), 2.45 (s, 4H), 4.70 (s, 1H), 7.19–7.29 (m, 4H); <sup>13</sup>C NMR (CDCl<sub>3</sub>, 75 MHz), δppm: 27.5, 29.4, 31.7, 32.4, 41.1, 50.8, 115.6, 128.6, 130.2, 132.4, 143.1, 162.5, 196.7.

### 3,3,6,6-Tetramethyl-9(4-nitro-phenyl)-1,8-dioxo-octahydroxanthene (Table 2, entry 3)

<sup>1</sup>H NMR (CDCl<sub>3</sub>, 300 MHz), δppm: 0.98 (s, 6H), 1.12 (s, 6H), 2.15 (d, *J*=16.3 Hz, 2H), 2.24 (d, *J*=16.3 Hz, 2H), 2.49 (s, 4H), 4.81 (s, 1H), 7.46 (d, *J*=7.9 Hz, 2H), 8.08 (d, *J*=7.9 Hz, 2H); <sup>13</sup>C NMR (CDCl<sub>3</sub>, 75 MHz), δppm: 27.2, 29.2, 32.3, 32.4, 40.8, 50.6, 114.5, 123.1, 129.3, 146.4, 151.5, 163.0, 196.3.

### 3,3,6,6-Tetramethyl-9(4-methoxy-phenyl)-1,8-dioxo-octahydroxanthene (Table 2, entry 6)

<sup>1</sup>H NMR (CDCl<sub>3</sub>, 300 MHz), δppm: 0.98 (s, 6H), 1.11 (s, 6H), 2.15 (d, *J*=15.7 Hz, 2H), 2.23 (d, *J*=15.7 Hz, 2H), 2.44 (s, 4H), 3.72 (s, 3H), 4.71 (s, 1H), 6.75 (d, *J*=8.6 Hz, 2H), 7.20 (d, *J*=8.6 Hz, 2H); <sup>13</sup>C NMR (CDCl<sub>3</sub>, 75 MHz), δppm: 27.4, 29.4, 31.2, 32.3, 40.8, 50.8, 55.1, 113.4, 115.8, 129.3, 136.5, 157.7, 162.0, 196.5.

## Conclusion

In this work, we have successfully synthesized a novel, effective and magnetic Fe<sub>3</sub>O<sub>4</sub>-PVP support chlorosulfonic acid as the catalyst for the preparation of xanthene derivatives through condensation of aldehydes and dimedone in ethanol at 80 °C. Clean reactions, simple performance, reusability of the nanocatalyst, easy

work-up method, high yield of products, and using  $\text{Fe}_3\text{O}_4\text{-PVP-SO}_3\text{H}$  as the powerful heterogeneous proton donor are outstanding advantages of this produced catalyst. It is worth mentioning that the catalyst has a wide surface area due to its nanospherical structure. Moreover, it was found to be potentially valuable in industrial applications and widespread use in organic synthesis for other compounds because of reusability of the magnetic heterogeneous nanocatalyst with maintaining its efficiency.

**Supplementary Information** The online version contains supplementary material available at <https://doi.org/10.1007/s11164-021-04542-3>.

**Acknowledgements** The authors acknowledge the financial support from Razi University of Kermanshah.

## References

1. S.M. Lee, E. Pippel, U. Gösele, C. Dresbach, Y. Qin, C.V. Chandran, T. Bräuniger, G. Hause, M. Knez, *Science* **324**, 488 (2009)
2. Z. Shao, F. Vollrath, *Nature* **418**, 741 (2002)
3. R.V. Lewis, *Chem. Rev.* **106**(9), 3762 (2006)
4. F.G. Omenetto, D.L. Kaplan, *Nat. Photonics* **2**, 641 (2008)
5. N. Lin, F. Hu, Y. Sun, C. Wu, H. Xu, X.Y. Liu, *Adv. Funct. Mater.* **24**, 5284 (2014)
6. J. Kim, Y. Piao, T. Hyeon, *Chem. Soc. Rev.* **38**, 372 (2009)
7. A. Nouri Parouch, N. Koukabi, E. Abdous, *Res. Chem. Intermed.* **46**, 3295 (2020)
8. M.H. So, Y. Liu, C.M. Ho, K.Y. Lam, C.M. Che, *ChemCatChem* **3**, 386 (2011)
9. G. Kandasamy, S. Soni, K. Sushmita, N.S. Veerapu, S. Bose, D. Maity, *J. mol. Liq.* **274**, 653 (2019)
10. M. Ozaki, *MRS Bull.* **14**, 35 (1989)
11. T. Neuberger, B. Schopf, H. Hofmann, M. Hofmann, B. von Rechenberg, *J. Magn. Magn. Mater.* **293**, 483 (2005)
12. C. Hui, C. Shen, J. Tian, L. Bao, H. Ding, C. Li, Y. Tian, X. Shi, H. J. Gao, *Nanoscale* **3**, 701 (2011)
13. P. Akbarzadeh, N. Koukabi, M.M. Hosseini, *J. Heterocyclic Chem.* **57**, 2455 (2020)
14. B. Karami, K. Eskandari, A. Ghasemi, *Turk. J. Chem.* **36**, 601 (2012)
15. X. Meng, W. Lei, W. Yang, Y. Liu, Y. Yu, *J. Colloid Interface Sci* **600**, 382 (2021)
16. G. Han, R. Sui, Y. Yu, L. Wang, M. Li, J. Li, H. Liu, W. Yang, *J. Magn. Magn. Mater.* **528**, 167824 (2021)
17. X. Liu, H. Liu, Y. Wang, W. Yang, Y. Yu, *J. Colloid Interface Sci.* **581**, 619 (2021)
18. S. Bao, W. Yang, Y. Wang, Y. Yu, Y. Su, *J. Hazard. Mater.* **409**, 124470 (2021)
19. X. Meng, Y. Liu, G. Han, W. Yang, Y. Yu, *Carbon*, **162**, 356 (2020)
20. M. Bagherzadeh, H. Haddadi, M. Iranpour, *Prog. Org. Coat.* **101**, 149 (2016)
21. D. Ling, M.J. Hackett, T. Hyeon, *Nano Today* **9**, 457 (2014)
22. G. T. Hermanson, *Bioconjugate techniques*. Academic press (2013)
23. Z. Shahedi, Y. Mansoori, *J. Part. Sci. Technol.* **4**, 67 (2018)
24. L. Shen, B. Li, Y. Qiao, *Mater.* **11**, 324 (2018)
25. S.T. Firdovsi, M. Yagoub, A.E. Parvin, *Chinese J. Chem.* **25**, 246 (2007)
26. K. Saravanan, B. Tyagi, H.C. Bajaj, *Catal. Sci. Technol.* **2**, 2512 (2012)
27. A.P. Kumar, J.H. Kim, T.D. Thanh, Y.I. Lee, *J. Mater. Chem. B.* **1**, 4909 (2013)
28. N.E. Leadbeater, M. Marco, *Chem. Rev.* **102**, 3217 (2002)
29. J. Liu, S.Z. Qiao, Q.H. Hu, G.Q. Lu, *Small* **7**, 425 (2011)
30. C. Shuai, W. Yang, C. He, S. Peng, C. Gao, Y. Yang, F. Qi, P. Feng, *Mater. Des.* **185**, 108275 (2020)
31. W. Yang, Y. Zhong, P. Feng, C. Gao, S. Peng, Z. Zhao, C. Shuai, *Polym. Test* **76**, 33 (2019)
32. C. Cheng, Y. Wen, X. Xu, H. Gu, *J. Mater. Chem.* **19**, 8782 (2009)
33. Y. Zhu, W. Zhao, H. Chen, J. Shi, *J. Phys. Chem. C* **111**, 5281 (2007)
34. A. Ruíz-Baltazar, R. Esparza, G. Rosas, R. Pérez, *J. Nanomater* **2015**, 240948 (2015)
35. M.A. Amin, K. Khaled, *Corros. Sci.* **52**, 1762 (2010)
36. H.H. Hassan, *Electrochim. Acta* **51**, 526 (2005)
37. S. Refaey, F. Taha, A.A. El-Malak, *Appl. Surf. Sci.* **242**, 114 (2005)

38. K.M. Koczkur, S. Mourdikoudis, L. Polavarapu, S.E. Skrabalak, Dalton Trans. **44**, 7883 (2015)
39. K. Seo, K. Sinha, E. Novitskaya, O.A. Graeve, Mater. Lett. **215**, 203 (2018)
40. O. Evangelinou, A.G. Hatzidimitriou, E. Velali, A.A. Pantazaki, N. Voulgarakis, P. Aslanidis, Polyhedron **72**, 122 (2014)
41. J.M. Khurana, D. Magoo, K. Aggarwal, N. Aggarwal, R. Kumar, C. Srivastava, Eur. J. Med. Chem. **58**, 470 (2012)
42. A. Jarrahpour, E. Ebrahimi, E.D. Clercq, V. Sinou, C. Latour, L.D. Bouktab, J.M. Brunel, Tetrahedron **67**, 8699 (2011)
43. A. Noack, H. Hartmann, Chem. Lett. **31**, 644 (2002)
44. J.F. Callan, A.P. De Silva, D.C. Magri, Tetrahedron **61**, 8551 (2005)
45. J. Liu, Z. Diwu, W.Y. Leung, Bioorg. Med. Chem. Lett. **11**, 2903 (2001)
46. S. Samantaray, P. Kar, G. Hota, B.G. Mishr, Ind. Eng. Chem. Res. **52**, 5862 (2013)
47. M.M. Khodaei, A. Alizadeh, H. Afshar Hezarkhani, Appl. Organometal. Chem. **34**, e5262 (2020)
48. M.M. Khodaei, A. Alizadeh, M. Haghipour, Res. Chem. Intermed. **46**, 1033 (2020)
49. M.M. Khodaei, M. Dehghan, Polyhedron **162**, 219 (2019)
50. M.M. Khodaei, A. Alizadeh, M. Haghipour, J. Organomet. Chem. **870**, 58 (2018)
51. M.M. Khodaei, M. Dehghan, New J. Chem. **42**, 11381 (2018)
52. Y. Zhu, W. Zhao, H. Chen, J. Shi, J. Phys. Chem. C. **111**, 5281 (2007)
53. S. Li, T. Zhang, R. Tang, H. Qiu, C. Wang, Z. Zhou, J. Magn. Magn. Mater. **379**, 226 (2015)
54. V.K. Baskrishnan, X. Han, G.W. VanLoon, J.M. Dust, J. Toullec, E. Buncel, Langmuir **20**, 6586 (2004)
55. L.Q. Pham, J.H. Sohn, C.W. Kim, J.H. Park, H.S. Kang, B.C. Lee, Y.S. Kang, J. Colloid Interface Sci. **365**, 103 (2012)
56. M. Bagherzadeh, O. Mousavi, Z. Shams Ghahfarokhi, New J. Chem. **44**, 15148 (2020)
57. C. Cui, Y. Du, T. Li, X. Zheng, X. Wang, X. Han, P. Xu, J. Phys. Chem. B. **116**, 9523 (2012)
58. S. Das, T. Dutta, R. Borah, J. Mol. Liq. **289**, 111099 (2019)
59. R. Mangalam, M. Thamilselvan, S. Selvasekarapandian, S. Jayakumar, R. Manjuladevi, Ionics **23**, 2837 (2017)
60. K. Mallick, M.J. Witcomb, M.S. Scurrell, Eur. Polym. J. **42**, 670 (2006)
61. H. Zhang, X. Zhong, J.J. Xu, H.Y. Chen, Langmuir **24**, 13748 (2008)
62. L. Wang, L. Wang, J. Luo, Q. Fan, M. Suzuki, I.S. Suzuki, M.H. Engelhard, Y. Lin, N. Kim, J.Q. Wang, C.J. Zhong, J. Phys. Chem. B **109**, 21593 (2005)
63. A. Hasaninejad, M. Dadar, A. Zare, Chem. Sci. Trans. **1**, 233 (2012)
64. Z.A. Piralghar, M.M. Hashemi, A. Ezabadi, Polycyclic Aromat. Compd. **40**, 1510 (2020)
65. F. Mohamadpour, M. Feilizadeh, Chem. Methodol. **4**, 647 (2020)
66. A. Zare, A.R. Moosavi-Zare, M. Merajoddin, M.A. Zolfigol, T. Hekmat-Zadeh, A. Hasaninejad, A. Khazaei, M. Mokhlesi, V. Khakyzadeh, F. Derakhshan-Panah, M.H. Beyzavi, E. Rostami, A. Arg-hoon, R. Roohandeh, J. Mol. Liq. **167**, 69 (2012)
67. P.J. Das, J. Das, RSC Adv. **5**, 11745 (2015)
68. A. Thakur, A. Sharma, A. Sharma, Synth. Commun. **46**, 1766 (2016)
69. H. Eshghi, M. Bakavoli, H. Moradi, Chin. Chem. Lett. **19**, 1423 (2008)
70. F. Nemat, S. Sabaqian, J. Saudi Chem. Soc. **21**, S383 (2017)

**Publisher's Note** Springer Nature remains neutral with regard to jurisdictional claims in published maps and institutional affiliations.